Title
In vivo evaluation of posterior eye elasticity using shaker-based optical coherence elastography

Journal
Experimental Biology and Medicine, 245(4)

ISSN
1535-3702

Authors
Qian, Xuejun
Li, Runze
Li, Yan
et al.

Publication Date
2020-02-01

DOI
10.1177/1535370219897617

Peer reviewed

Original Research

In vivo evaluation of posterior eye elasticity using shaker-based optical coherence elastography

Xuejun Qian[1,2,*], Runze Li[1,2,*], Yan Li[3], Gengxi Lu[1,2], Youmin He[3], Mark S Humayun[1,2], Zhongping Chen[3] and Qifa Zhou[1,2]

[1]Department of Biomedical Engineering and NIH Ultrasonic Transducer Resource Center, University of Southern California, Los Angeles, CA 90089, USA; [2]USC Roski Eye Institute, University of Southern California, Los Angeles, CA 90033, USA; [3]Beckman Laser Institute, University of California, Irvine, Irvine, CA 92612, USA

Corresponding authors: Zhongping Chen. Email: z2chen@uci.edu; Qifa Zhou. Email: qifazhou@usc.edu

*These authors contributed equally to this work.

Impact statement

Herein, we propose a potentially clinical applicable shaker-based optical coherence elastography (OCE) technique to characterize the biomechanical properties of the posterior eye, including different layers of the retina. Compared with either acoustic radiation force OCE or air-puff OCE, the newly developed method can induce sufficient shear wave propagation at the posterior eye with high resolution and large field of view.

Abstract

Age-related macular degeneration (AMD) is a progressive retinal disease and becomes the leading cause of blindness. It is well established that early detection is the key to preservation of functional vision. However, it is very difficult to diagnose AMD in very early stages, before structural changes are evident. Consequently, investigating the biomechanical properties of the retina maybe essential for understanding its physiological function. In this study, we present a shear wave-based quantitative method for estimating the elasticity of the posterior eye using shaker-based optical coherence elastography. This technique has been developed and validated on both a homogeneous phantom and a healthy rabbit *in vivo*. The shear wave speed from the ganglion side to the photoreceptor side of the rabbit eye is 4.1 m/s, 4.9 m/s, and 6.7 m/s, respectively. In addition, the most stiff sclera region has an average shear wave speed of 9.1 m/s. The results demonstrate the feasibility of using this technique to quantify biomechanical properties of the posterior eye and its potential translation to the clinical study.

Keywords: Shear wave elastography, optical coherence tomography, posterior eye elasticity

***Experimental Biology and Medicine* 2020; 245: 282–288. DOI: 10.1177/1535370219897617**

Introduction

Retinal diseases, such as age-related macular degeneration (AMD) are the leading cause of severe, irreversible vision loss in people aged over 60.[1] It has been shown that the main cause for visual loss in AMD is the development of choroidal neovascularization (CNV). Although there are available treatments for CNV, they are not capable of reversing the injury nor able to improve vision in the majority of cases.[2] As a result, early detection is the key to preservation functional vision.

To understand the pathogenesis of the AMD, several ocular imaging technologies have been developed for the purpose of AMD detection and monitoring. The first transformative imaging was the invention of fluorescein angiography to visualize the vessel distribution/blood leakage if neovascularization is suspected.[3] Later, another imaging modality namely fundus photography has been developed on epidemiological studies of AMD to establish major risk factors.[4,5] More recently, a new imaging modality referring to optical coherence tomography (OCT)[6] has been introduced to provide better visualization of the various retinal layers non-invasively. Despite these techniques are capable of providing crucial information for the diagnosis of AMD, they often are insufficient for early diagnosis, before structural changes occur. It recently has been shown that the mechanical properties of distinct cellular layers in the retina are altered with the onset of AMD.[7] Thus, investigating the biomechanical properties of the posterior eye, especially retina, is essential for

understanding its physiological function and their response to stress from injuries, medical device implantation, and potential surgeries.

Elastography, an imaging modality capable of mapping the biomechanical properties of soft tissues, provides additional contrast mechanism and clinically relevant information for disease diagnosis. A typical elastography imaging system is composed of two parts: excitation and detection. Compared with conventional ultrasound elastography,[8] high frequency ultrasound elastography[9,10] and magnetic resonance elastography,[11] utilizing optical coherence elastography (OCE) as the detection method, have gained the capability to characterize subtle stiffness changes in ocular tissue because of the high resolution (<10 μm) and the advantage in transparency.[12,13]

To induce a small temporal axial displacement to launch a mechanical shear wave in ocular tissue, multiple excitation methods have been explored, including air-puff,[14,15] acoustic micro-tapping,[16] and acoustic radiation force (ARF).[17–19] To be specific, current air-puff OCE was focused on producing mechanical waves in the cornea and has not been applied on the posterior eye. In addition, air-puff pulse suffers from few limitations, including the low bandwidth of the induced mechanical waves and slow relaxation times.[12] Another excitation approach is so-called acoustic micro-tapping. In general, a spatially and temporally sharp pressure is applied to the tissue surface via a focused air-coupled ultrasound transducer. Because a major part of the acoustic intensity is reflected at the boundary, only less than 1% intensity was applied to the tissue, launching a wave with nano to micrometer displacement. Owing to the stiff sclera tissue and large attenuation from the long propagation distance to posterior eye, the feasibility of applying this approach to characterize the elasticity of posterior eye still needs further investigation. In order to have a more controllable localized force inside the imaging region, Qu *et al.*[20] first applied ARF-OCE technique to characterize the biomechanical properties of the retina *in vivo* and successfully reconstructed the elasticity of each retinal layer. However, owing to the large acoustic attenuation of the anterior chamber, especially of the lens, a high power ARF is typically desired to induce sufficient deformation at the posterior eye directly. As a consequence, its mechanical index (MI) and acoustic intensity remain a challenge to meet the strict U.S Food and Drug Administration (FDA) standards for ophthalmic exposure.

In this study, we report on the development of a shaker-based OCE technique as a potential tool for clinical study. The proposed method has the capability to assess the elasticity of the posterior eye, including different layers of the retina via shear wave elastography. The performance of the system has been validated on both a homogeneous phantom and a healthy rabbit eye *in vivo*.

Materials and methods

Experimental setup

A schematic diagram of the experimental setup is shown in Figure 1. To induce the shear wave, a mechanical shaker (mini-shaker type 4810; Bruel & Kjaer, Duluth, Georgia, USA) was positioned at the anterior sclera which is close to corneal limbus via a contact rod. The tip of the rod has a square shape with the size of 1.2 mm by 1.2 mm. Then, the shaker was aligned along the scanning direction of the OCT beam.

To precisely track the tissue motion caused by mechanical shaker, a customized 50 kHz spectral domain optical

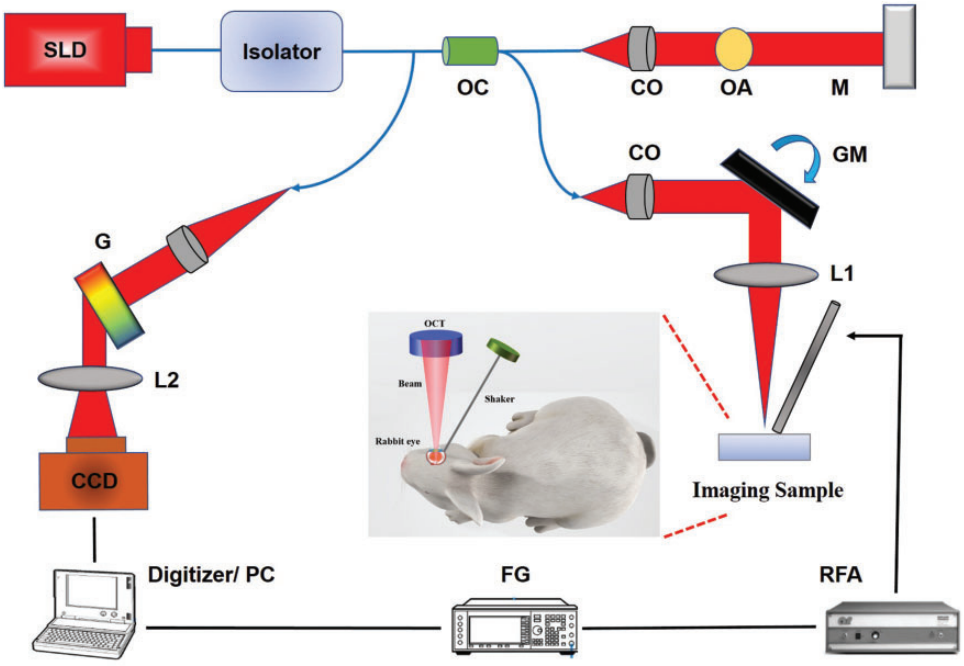

Figure 1. Shaker-based OCE system schematic diagram with *in vivo* rabbit eye setup. SLD: superluminescent diode: OC: optical coupler: CO: collimator: OA: optical attenuator: M: mirror: GM: galvanometer mirrors: L1/L2: lens: RFA: radiofrequency amplifier: FG: function generator: G: grating. (A color version of this figure is available in the online journal.)

coherence tomography (SD-OCT) system with a central wavelength of 890 nm and bandwidth of 144 nm was built. For the safety purpose, the light beam was filtered through an optical isolator (IO-F-SLD150-895, Thorlabs Inc., Newton, NJ, USA) and then split 20% to the imaging sample and 80% to a reference mirror using an optical coupler. Glass imaging windows are placed in the stationary reference arm for dispersion compensation. During the experiment, the scattering signal from the sample arm is first coupled together with the reflected reference arm signal, and then generates the interference signal. Next, the signal is separated by wavelength with a diffraction grating and focused onto a line scan CMOS camera. Finally, the raw signals were saved offline for further processing. For the purpose of the shear wave tracking, the shaker was fixed, while galvo mirrors scan at M-B mode with a step size of 6 μm. A total of 3 mm scanning distance was acquired.

To synchronize the shaker and the SD-OCT detection system, the PC sent out a baseline signal to trigger the arbitrary function generator (AFG 3252 C, Tektronix, Beaverton, OR, USA), which generates an impulse signal with a pulse width from 200 μs to 1 ms. Then the impulse signal was transmitted to a power amplifier (Type 2718, Bruel & Kjaer, Duluth, Georgia, USA) to generate an amplified impulse signal to the mechanical shaker to induce tissue deformation. At each lateral scanning location, M-mode collected a total of 400 A-lines, corresponding to the time of 8.8 ms, before the galvanometer moves to the next scanning position. To establish the baseline for the displacement curve, the mechanical shaker was excited to 100 μs after the SD-OCT system started to acquire data. These parameter settings were kept constant for both phantom study and *in vivo* animal study.

Post-processing and data analysis

Data analysis was performed using MATLAB. The signal is processed and transformed into depth-resolved intensity and phase-resolved displacement.

To calculate the shear wave speed (SWS), the spatiotemporal map (lateral distance versus time shifts curve) was obtained from the axial displacement map where the lateral distance was measured by the moving step size of the galvo mirror and the time shift (defined as the time to reach the peak displacement at each dynamic displacement). Then, the SWS was estimated by applying a linear regression to all peak displacement points along successive lateral locations. To quantify the Young's modulus, we used the equation $E = 3 \cdot \rho \cdot c_s^2$ where ρ presents the tissue density (approximately 1 kg/m^3) and c_s is the SWS.

Phantoms and rabbit preparation

A custom-built silicone phantom was first fabricated to test the performance of the system. The stiffness of the homogeneous phantom was tested by the gold-standard – uniaxial mechanical testing (Model 5942, Instron Corp., MA, USA), which is equal to 73.9 ± 7 kPa.

The *in vivo* rabbit experiment was performed according to the University of Southern California Institutional Animal Care and Use Committee (IACUC) protocol. Dutch belted pigmented rabbit (~2 kg) was single housed and fed with normal diet. Prior to the imaging experiment, the rabbit was anesthetized with ketamine (35 mg/kg) and xylazine (5 mg/kg) via subcutaneous injection. Two drops of phenylephrine were applied topically to prevent cornea swelling and decrease discomfort. Redosing of anesthesia was achieved by 2.5% sevoflurane through a facial mask. The heart rate, respiratory, body temperature, oxygen saturation, and non-invasive blood pressure were recorded every 5 min until it became fully conscious.

Results

Phantom results

The shaker was positioned at 4.8 mm laterally away from the OCT detection beam in order to mimic the potential shear wave propagation distance from anterior sclera to posterior segment of the eye. Figure 2(a) shows the displacement curves under the 200 μs, 600 μs, and 1000 μs shaker duration which was acquired at the initial galvo position, respectively. It was observed that longer duration provides better signal-to-noise (SNR) ratio. However, for the purpose of safety and maintaining a wide bandwidth of the generated shear wave, 600 μs was selected as a balance and further implemented for the *in vivo* rabbit study. Figure 2(b) shows the displacement curves at three different depths of the phantom. It was observed that the peak displacement and the time to reach the peak displacement

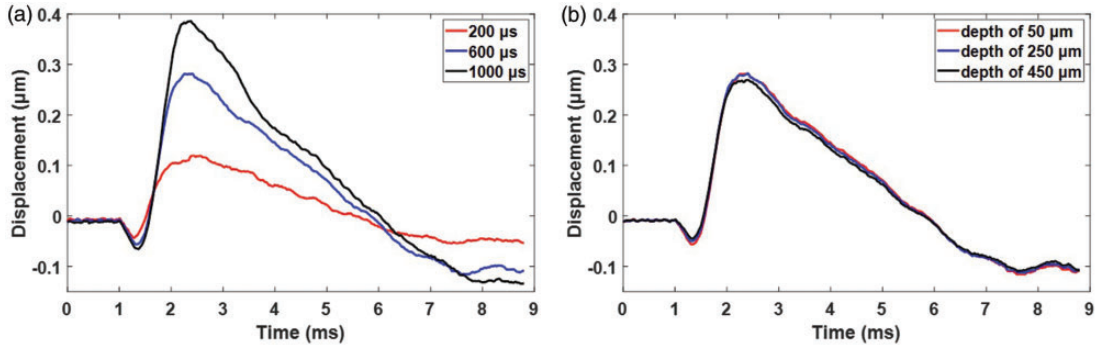

Figure 2. Displacement curves of the homogeneous phantom. (a) With 200 μs, 600 μs, and 1000 μs shaker pulse duration at the initial galvo position (the most left position of the OCT image). (b) At the depth of 50 μm, 250 μm, and 450 μm under the condition of 600 μs shaker pulse duration. (A color version of this figure is available in the online journal.)

are similar among three depths, indicating the uniform force distribution in axial direction.

Figure 3(a) to (c) shows the OCT image, spatiotemporal map, and shear wave propagation at three different time points, respectively. The effective field of view (FOV) of shaker-based OCE system can reach up to 600 μm, and therefore it is sufficient to cover the imaging subject where the healthy rabbit retinal thickness averages about 300–400 μm. To assess the accuracy of our proposed shaker-based OCE method on estimating Young's modulus, we compared it with the gold standard – uniaxial mechanical testing (Instron 5942). Calculated from the spatiotemporal displacement map of the phantom, the SWS determined by the linear regression of the ratio between the propagation distance and the time to reach the peak displacement in successive lateral locations is 5.1 ± 0.3 m/s, corresponding to the Young's modulus of 78.3 ± 9 kPa. The calculated Young's modulus is consistent with 73.9 ± 7 kPa tested on gold standard. The difference between the reconstructed Young's modulus via SWS and the gold standard is not significant (P value $= 0.4133$, where $P < 0.05$ is considered to be significantly different), and is within the acceptable range of error (~5%).

It was also observed in Figure 2 that the first 1 ms in axial displacement curve at the initial galvo position has no displacement, which corresponds to the propagation time from the location of shaker to the region of interest (ROI) of the phantom plus the synchronization delay between shaker and SD-OCT system. By removing the synchronization delay time, we got the pure shear wave propagation time of 900 μs. As a result, the average SWS in this region was estimated to be 5.3 m/s, which is close to the calculated 5.1 m/s inside the OCT beam scanning region. All these results demonstrated that our imaging method has the capability to assess the Young's modulus precisely.

In vivo rabbit posterior eye

Imaging was performed on the central retina and the same M-B mode scanning scheme was used to capture the shear wave propagation. The structural resliced OCT images were obtained as shown in Figure 4(a), where the individual five posterior layers of the eye could be isolated. Figure 4(b) to (d) shows the shear wave propagation at time of 0, 0.088, and 0.176 ms, respectively. In Figure 5(a) to (d), four spatiotemporal displacement maps at layers 1, 2, 3, and 5 (indicated in the Figure 4(a)) are plotted, respectively. The SWS of the first three layers from the ganglion side to the photoreceptor side are: 4.1 m/s, 4.9 m/s, and 6.7 m/s, which are corresponding to the elasticity of 50.4 kPa, 72 kPa, and 134.6 kPa, respectively. Owing to the low OCT signal in layer 4, the SWS of the choroid was not identified here. The layer 5 – sclera has an average SWS of 9.1 m/s which corresponds to the elasticity of 248 kPa.

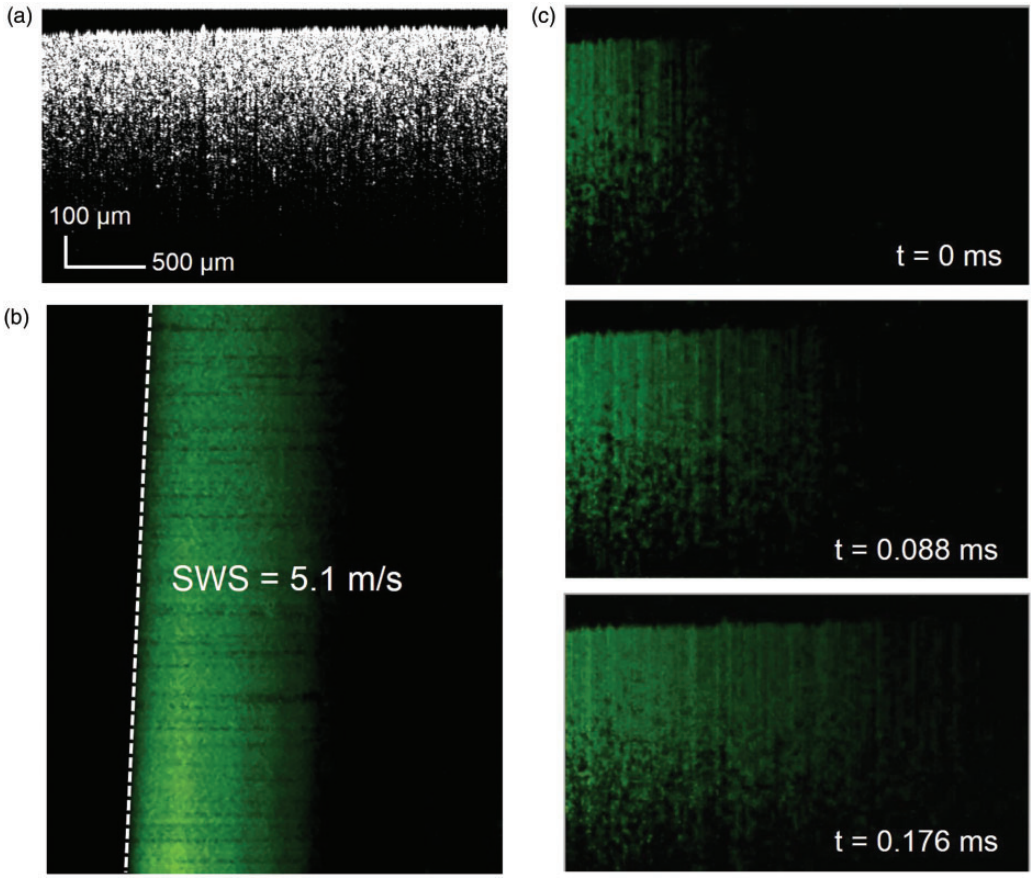

Figure 3. (a) OCT image of the phantom, (b) spatiotemporal displacement map of the homogeneous phantom, (c) shear wave propagation at the timing of 0, 0.088, 0.176 ms, respectively.

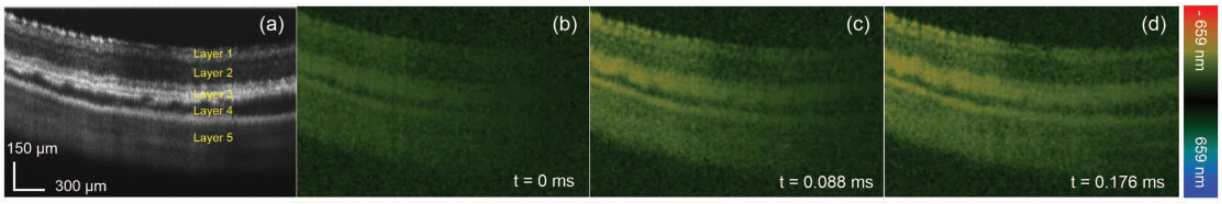

Figure 4. (a) OCT image of the posterior rabbit eye *in vivo*, (b–d) shear wave propagation maps at the timing of 0, 0.088, 0.176 ms, respectively. Layer 1: Nerve fiber, ganglion cell, and inner plexiform; Layer 2: inner nuclear, outer plexiform, and outer nuclear; Layer 3: RPE; Layer 4: choroid; Layer 5: sclera.

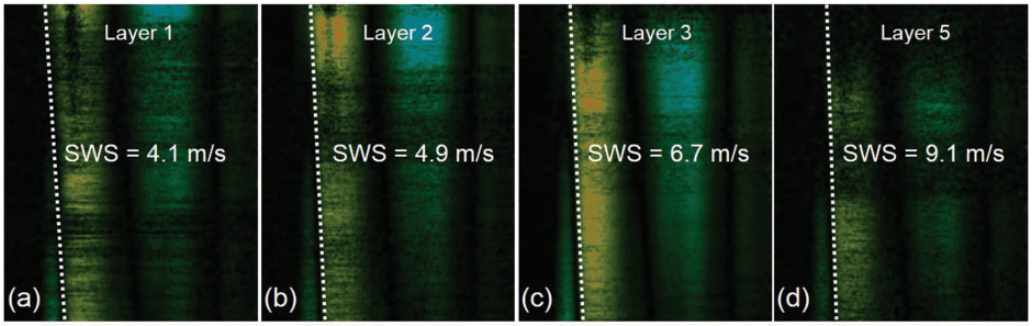

Figure 5. Spatiotemporal displacement maps of different layers of the posterior eye. (a) Layer 1, (b) Layer 2, (c) Layer 3, and (d) Layer 5.

Discussion

Optical coherence tomography is a well-developed imaging technique to provide excellent spatial resolution and can be used to characterize the tissue biomechanical properties when combined with an external inducing force. In recent years, quantified elasticity maps of the *in vivo* posterior eye are first presented by using ARF-OCE technique. However, ARF-based technique suffers from two concerns. One is non-uniform ARF beam and relative shallow ARF excitation region in the axial direction; another concern is the safety issue. The mechanical index (MI) for ocular applications is 0.23 as determined by the FDA. In order to maintain a high SNR, a large output power of ARF is typically required, which impedes its translation to clinical studies. By contrast, shaker-based method has been previously investigated by ultrasound elastography studies on human subjects in clinic, including cornea[21] and posterior sclera,[22] which may be a relatively safe approach.

In this study, we used a shaker to mechanically induce the tissue deformation. To be specific, the force is applied orthogonally to the anterior sclera surface in order to provide shear wave propagation only.[23] As indicated by Palmeri *et al.*,[24] the frequency bandwidth of phase velocity depends on the excitation duration and spatial beamwidth used to generate the shear wave. Excitation durations from 100 to 700 μs (less than 1 ms) are typically used to induce shear wave propagation.[25] Based on these previous studies, we concluded that shorter excitation duration can obtain wider shear wave bandwidth, resulting in more accurate estimation of elasticity. However, previous ARF-OCE system utilized a relative long ARF excitation duration. This is because that a short excitation duration (below 1 ms) would not induce enough detectable displacement at posterior eye, especially when the shear wave propagates far away from the region of excitation of the pushing transducer.[20,26] Compared with ARF method, the minimally contact shaker method is capable of providing a shorter pushing duration – 600 μs is used in this study, while maintaining sufficient tissue deformation.

The performance of the shaker-based OCE system was first validated on a homogeneous phantom. The variance of the peak displacements among different axial depths in Figure 2(b) is less than 5%, which implies that the shaker has the potential to generate uniform force distribution within the OCT image view. In addition, the Young's modulus of the phantom reconstructed by the linear regression of the peak displacement points in the spatiotemporal map is closely relative to the mechanical testing results. All these results demonstrated that the shaker-based OCE has the ability to accurately capture the shear wave propagation with a large field of view. To further validate the potential capability of our system on pre-clinical *in vivo* study, the posterior rabbit eye was imaged.

There are few literature studies on the elasticity range of the posterior eye. Chen *et al.*[27] identified the elastic modulus of the retina *ex vivo* using mechanical testing. However, this test is performed on porcine tissue and without perturbing the natural retinal environment. Qu *et al.*[20] first demonstrated the mechanical quantification of the *in vivo* posterior eye using the bulk frequency response method. In a healthy rabbit model, their mechanical properties vary from 3 to 16 kPa in different layers of the retina. However, the measured biomechanical properties depend on many parameters such as test conditions, species, and most importantly, measurement technique. The resonance frequency-based elasticity measurement is highly dependent on the characterization of the tissue and the implemented model. Later, He *et al.*[26] reconstructed the elasticity of the retina using shear wave OCE. In their

report, the elasticity of the first three layers from the ganglion side to the photoreceptor side ranges from 12 kPa to 101 kPa. In addition, they indicated that the Young's modulus of the bottom two layers is over 100 kPa. Our calculated Young's modulus from anterior retina to posterior retina and sclera are in a reasonable range compared with results above.

In this study, we successfully demonstrate the capability of our imaging system to characterize the biomechanical properties of the posterior eye. Considering the high safety requirements in clinical study, our shaker-based OCE system may have the translational potential for clinical diagnosis. However, a few challenges remain to be addressed before the technology can be translated. First, the group velocity-based elasticity assessment in this study maybe inaccurate (i.e. under the assumption of pure elasticity and homogeneous medium) and may lead to some bias because of boundary conditions and the ratio of retina thickness to shear wavelength. A multi-layer model (modified from previously developed Lamb wave model[23]) is needed to precisely reconstruct both elasticity and viscosity of different retinal layers. Second, as suggested by Kirby *et al.*,[12] the bandwidth of generated mechanical waves depends on the temporal and spatial characteristics of the excitation push. Although 600 μs is a short push, the push cross section determined by the size of shaker's contact rod is not tiny in this study, which may reduce the mechanical wave bandwidth. They also pointed out that the bandwidth/wavelength relationship of the mechanical wave determines the spatial resolution of reconstructed elastic modulus maps. In the future study, a tiny rod will be implemented, which may help us to further characterize the reconstructed elastic modulus maps. Finally, the safety issue of the shaker-induced process still needs to be further investigated to ensure its potential applications in clinical settings.

Conclusions

In summary, we demonstrate that the shaker-based OCE method has the ability to accurately map the biomechanical properties of different retinal layer and sclera underneath. Compared with ARF-OCE approach, our developed method can induce sufficient shear wave propagation at the posterior eye with high resolution and large field of view, which could lead to a quicker clinical uptake.

Authors' contributions: XQ and RL conducted experiments, collected, and analyzed data. YL, YH provided the technical support. XQ, RL, and GL wrote the manuscript. MH, ZC, and QZ initiated and designed the study. All authors contributed to the review and editing of the manuscript.

DECLARATION OF CONFLICTING INTERESTS

Dr. Z.C. has a financial interest in OCT Medical Imaging Inc., which, however, did not support this work. All other authors declared no potential conflicts of interest.

FUNDING

This work was supported by the National Institutes of Health (NIH) under grant R01EY026091, R01EY028662, R01EY030126, R01CA211602 and NIH P30EY029220. Unrestricted departmental grant from research to prevent blindness.

ORCID iD

Xuejun Qian https://orcid.org/0000-0003-3634-8757

REFERENCES

1. Jager RD, Mieler WF, Miller JW. Age-related macular degeneration. *N Engl J Med* 2008;**358**:2606–17
2. Loewenstein A. The significance of early detection of age-related macular degeneration: Richard & Hinda Rosenthal foundation lecture, the macula society 29th annual meeting. *Retina* 2007;**27**:873–8
3. Novotny HR, Alvis DL. A method of photographing fluorescence in circulating blood in the human retina. *Circulation* 1961;**24**:82–6
4. Connell PP, Keane PA, O'Neill EC, Altaie RW, Loane E, Neelam K, Nolan JM, Beatty S. Risk factors for age-related maculopathy. *J Ophthalmol* 2009;**360764**:39 pages
5. Group A-REDSR. The age-related eye disease study system for classifying age-related macular degeneration from stereoscopic color fundus photographs: the age-related eye disease study report number 6. *Am J Ophthalmol* 2001;**132**:668–81
6. Hee MR, Baumal CR, Puliafito CA, Duker JS, Reichel E, Wilkins JR, Coker JG, Schuman JS, Swanson EA, Fujimoto JG. Optical coherence tomography of age-related macular degeneration and choroidal neovascularization. *Ophthalmology* 1996;**103**:1260–70
7. Krishnan L, Hoying JB, Nguyen H, Song H, Weiss JA. Interaction of angiogenic microvessels with the extracellular matrix. *Am J Physiol* 2007;**293**:H3650–H58
8. Detorakis ET, Drakonaki EE, Tsilimbaris MK, Pallikaris IG, Giarmenitis S. Real-time ultrasound elastographic imaging of ocular and periocular tissues: a feasibility study. *Ophthalmic Surg Lasers Imaging* 2010;**41**:135–41
9. Qian X, Ma T, Yu M, Chen X, Shung KK, Zhou Q. Multi-functional ultrasonic micro-elastography imaging system. *Sci Rep* 2017;**7**:1230
10. Qian X, Ma T, Shih C-C, Heur M, Zhang J, Shung KK, Varma R, Humayun MS, Zhou Q. Ultrasonic microelastography to assess biomechanical properties of the cornea. *IEEE Trans Biomed Eng* 2018;**66**:647–55
11. Litwiller DV, Lee SJ, Kolipaka A, Mariappan YK, Glaser KJ, Pulido JS, Ehman RL. MR elastography of the ex vivo bovine globe. *J Magn Reson Imaging* 2010;**32**:44–51
12. Kirby MA, Pelivanov I, Song S, Ambrozinski L, Yoon SJ, Gao L, Li D, Shen TT, Wang RK, O'Donnell M. Optical coherence elastography in ophthalmology. *J Biomed Opt* 2017;**22**:121720
13. Larin KV, Sampson DD. Optical coherence elastography – OCT at work in tissue biomechanics. *Biomed Opt Express* 2017;**8**:1172–202
14. Li J, Wang S, Singh M, Aglyamov S, Emelianov S, Twa M, Larin K. Air-pulse OCE for assessment of age-related changes in mouse cornea in vivo. *Laser Phys Lett* 2014;**11**:065601
15. Wang S, Li J, Manapuram RK, Menodiado FM, Ingram DR, Twa MD, Lazar AJ, Lev DC, Pollock RE, Larin KV. Noncontact measurement of elasticity for the detection of soft-tissue tumors using phase-sensitive optical coherence tomography combined with a focused air-puff system. *Optics Lett* 2012;**37**:5184–6
16. Ambroziński Ł, Song S, Yoon SJ, Pelivanov I, Li D, Gao L, Shen TT, Wang RK, O'Donnell M. Acoustic micro-tapping for non-contact 4D imaging of tissue elasticity. *Sci Rep* 2016;**6**:38967
17. Qi W, Chen R, Chou L, Liu G, Zhang J, Zhou Q, Chen Z. Phase-resolved acoustic radiation force optical coherence elastography. *J Biomed Opt* 2012;**17**:110505
18. Nguyen T-M, Arnal B, Song S, Huang Z, Wang RK, O'Donnell M. Shear wave elastography using amplitude-modulated acoustic radiation

force and phase-sensitive optical coherence tomography. *J Biomed Opt* 2015;**20**:016001
19. Mikula E, Hollman K, Chai D, Jester JV, Juhasz T. Measurement of corneal elasticity with an acoustic radiation force elasticity microscope. *Ultrasound Med Biol* 2014;**40**:1671–9
20. Qu Y, He Y, Saidi A, Xin Y, Zhou Y, Zhu J, Ma T, Silverman RH, Minckler DS, Zhou Q. In vivo elasticity mapping of posterior ocular layers using acoustic radiation force optical coherence elastography. *Invest Ophthalmol Vis Sci* 2018;**59**:455–61
21. Sit AJ, Lin S-C, Kazemi A, McLaren JW, Pruet CM, Zhang X. In vivo noninvasive measurement of young's modulus of elasticity in human eyes: a feasibility study. *J Glaucoma* 2017;**26**:967–73
22. Zhou B, Chen JJ, Kazemi A, Sit AJ, Zhang X. An ultrasound vibro-elastography technique for assessing papilledema. *Ultrasound Med Biol* 2019;**45**:2034–9
23. Shih C-C, Qian X, Ma T, Han Z, Huang C-C, Zhou Q, Shung KK. Quantitative assessment of thin-layer tissue viscoelastic properties using ultrasonic micro-elastography with lamb wave model. *IEEE Trans Med Imaging* 2018;**37**:1887–98
24. Palmeri ML, Deng Y, Rouze NC, Nightingale KR. Dependence of shear wave spectral content on acoustic radiation force excitation duration and spatial beamwidth. In: *The annual 2014 IEEE International Ultrasonics Symposium will be held at the Hilton Hotel*, Chicago, IL, USA, 3–6 September 2014.
25. Widman E, Maksuti E, Amador C, Urban MW, Caidahl K, Larsson M. Shear wave elastography quantifies stiffness in ex vivo porcine artery with stiffened arterial region. *Ultrasound Med Biol* 2016;**42**:2423–35
26. He Y, Qu Y, Zhu J, Zhang Y, Saidi A, Ma T, Zhou Q, Chen Z. Confocal shear wave acoustic radiation force optical coherence elastography for imaging and quantification of the in vivo posterior eye. *IEEE J Select Topics Quantum Electron* 2018;**25**:1–7
27. Chen K, Rowley AP, Weiland JD. Elastic properties of porcine ocular posterior soft tissues. *J Biomed Mater Res Part A* 2010;**93**:634–45

(Received September 16, 2019, Accepted October 29, 2019)